PCCP

Regular microscopic patterns produced by simple reaction–diffusion systems

Péter Hantz

Department of Theoretical Physics, Eötvös University, Department of Physical Chemistry, Eötvös University, Pázmány sétány 1/A, H-1117, Budapest, Hungary, and Department of Plant Taxonomy and Ecology, Eötvös University, Pázmány sétány 1/C, H-1117, Budapest, Hungary. E-mail: hantz@poe.elte.hu

Received 28th August 2001, Accepted 23rd November 2001
First published as an Advance Article on the web

Simple inorganic reactions, coupled with diffusion, are able to produce regular patterns of characteristic length scales of 10 μm. Solutions of $CuCl_2$ or $AgNO_3$ are homogenised in poly(vinyl)alcohol gel, and NaOH is allowed to diffuse into the gel. Reaction of the NaOH solution with the electrolyte present in the gel forms precipitates, which can show several types of primary (macroscopic) patterns, including spirals and target-like patterns. Depending on the velocity of the reaction front, the colloidal precipitate developed in this chemical reaction can yield a microscopic structure consisting of ordered sheets of particles. Conditions of formation and characterisation of the secondary (microscopic) patterns are presented. Emergence and disappearance of defects in these structures are also investigated. Possible theoretical explanation and technological applications of the microscopic patterns are discussed.

Introduction

Reaction–diffusion processes have a fundamental role in pattern formation of several biological and chemical systems.[1–12] A large number of chemical systems have been tested to find out whether they can yield fine patterns, which can be useful in technological processes. Up to now, the characteristic size of the finest stable structures produced by chemical reaction–diffusion systems was of the order of millimetres.[13] These patterns were produced by the Liesegang phenomenon, where colloidal precipitate forms behind a moving reaction front.[13–16] However, diffusion-controlled reactions in solids can lead to periodic banding having wavelength of the order of 10 μm. These bands of particles are located in a continuous intermetallic matrix phase.[17]

Surprising properties of the NaOH + $CuCl_2$ reaction have been described recently.[18] This simple reaction exhibits most of the important patterns, that until now have only been observed in much more complicated chemical systems.[2,3] Liesegang rings, spiral-shaped interacting chemical fronts and, at higher concentrations, irregular patterns were obtained. These structures will be referred to from now as primary, macroscopic patterns. A more careful look at the CuO precipitate formed in this process revealed that under certain circumstances this substance may have a regular microscopic structure that is composed of parallel sheets of colloidal precipitate. These microscopic structures will be referred to from now as secondary patterns.

The aim of this work was to study experimentally the secondary patterns, and to give a possible theoretical interpretation of the results.

Sample preparation

Two series of experiments have been performed, either in gel sheets or in gel columns. The gel was made as follows: 8.6 w/w % poly(vinyl)alcohol (PVA) solution was prepared by adding PVA powder (PVA 72000, Merck Z.S.) to high-purity water (supplied by Labconco and Millipore filter series) under continuous stirring at 70–80 °C. Complete solubilisation was achieved by stirring for 4 h at this temperature, and then allowing to cool to room temperature. Inner electrolytes of the required concentrations were obtained by adding different amounts of $CuCl_2$ (Merck A.R.) solutions to a series of PVA solutions, each of 100.0 mL. Acidity and cross-linking of the gel were set by adding 2.00 mL of 18.50 w/w % HCl (Reanal A.R.) and 1.00 mL of 1.0 M glutaraldehyde (Merck Z.S) to the above mixtures, then high-purity water was used to top up each solution to 200.0 mL. After a strong mixing, the air bubbles were driven out by putting the solution into an ultrasonic device for 10–20 s.

To prepare experiments in gel sheets, 2–3 droplets of the above solution were placed on a microscope slide, and covered with a cover glass of 22×32 mm. After 1–3 h, while the gelation took place, the reactions were started by placing 4–5 droplets of 8.0 M NaOH outer electrolyte solution (Reanal A.R.) on one of the edges of the gel sheet, and covering with a cover glass to avoid evaporation. For the experiments in gel columns the solutions were poured into glass test tubes of 14 mm inner diameter to a height of 100–120 mm. After 10–20 h the reaction was started by pouring 6.00 mL of NaOH outer electrolyte onto the top of the gel columns. The experiments were carried out at room temperature.

Experiments in gel sheets

In order to study details of the formation of the secondary patterns, the reaction was started in thin gel sheets and followed by optical microscope. PVA gel containing 0.732 M $CuCl_2$ was located between a slide and a cover glass, and 8.0 M NaOH solution was allowed to diffuse into the gel from the edge of the gel sheet. In this way a one-dimensional diffusion front was formed (Fig. 1a).

DOI: 10.1039/b107742b

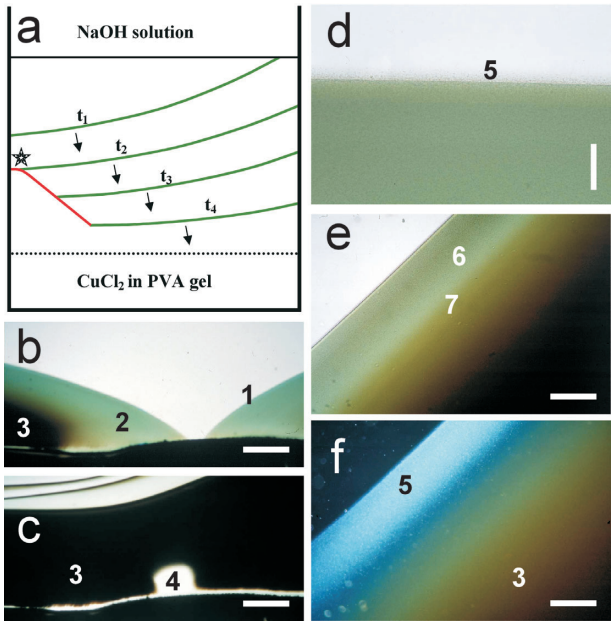

Fig. 1 (a) Formation of a passive edge. The black dots represent the diffusion front of the NaOH, the green curves the sweeping reaction zone at different times, and the red curve the passive edge. The point where the formation of the precipitate is halted, is marked by an asterix. (b) Two approaching reaction fronts (1) before they meet. The green precipitate (2) can be observed behind them. No A-type colloids are present at the reaction fronts. The brown CuO colloid (3) emerged in the regions where the front swept 7–8 min earlier. Thicker layers of the brown precipitate look black. Scale bar = 800 μm. (c) The same scenario after the reactions have taken place. The place where the reaction front swept through is thickly filled with the brown precipitate (3), except in region (4), next to the meeting point, where the front velocity was higher than about 2.1 μm s^{-1}. Scale bar = 800 μm. (d) Homogeneous A-type precipitate (5) emerged just before the reaction front. Scale bar = 50 μm. (e) Decay of the A-type (6), and emergence of the brown (7) precipitate. Scale bar = 200 μm. (f) The same patterns in dark-field investigation. The A-type precipitate shines in white (5), while the brown one in brown (3). Scale bar = 200 μm.

The diffusion front of the NaOH cannot be observed by ordinary optical microscopy. Behind this diffusion front there is a region, where both reactants are present. This area is referred to as the excitable region, *i.e.* a place where pattern formation can occur. Inside this region can arise and move sharp reaction fronts or reaction zones (Fig. 1a), where a precipitate is formed that looks green in transmitted light, and shows no structure when investigated with optical microscopy. The dynamics of the formation and interactions of reaction fronts, which determine the structures of the primary, macroscopic patterns, have been discussed in detail.[18] A main feature is the formation of so-called passive edges. Fig. 1a shows how a passive edge can emerge. At a point on the reaction front, usually at the border of the gel sheet, the formation of the structureless precipitate is halted. As the reaction front advances, these points expand into empty regions free of this precipitate. The borders of these empty regions are referred to as passive edges. These borders are stationary, but new reaction fronts can form on them. A mathematical model which reproduces the main characteristics of this dynamics has been elaborated and will be presented in a forthcoming article.[19] Note, that these breaks in the fronts have some common aspects with those that were reported in ref. 20.

The velocity of the reaction front is mainly determined by the speed of the diffusion front and the shape of the reaction front. The velocity of the diffusion front decreases with time, roughly by a square-root law. When a new reaction front emerges, after a transient period with greater velocity, its speed becomes diffusion-limited. The shape of the front is also important. The speed of a convex segment of a reaction front is less than that of a straight one, and a straight segment's velocity is less than that of a concave front. This behaviour is in agreement with the predictions of the kinematical theory of chemical waves.[21] Velocity plays an essential role in determining which kinds of secondary, microscopic patterns are formed as the front advances. The secondary patterns consist of various kinds of colloidal precipitates.

The main characteristics of the patterns that emerge at various front velocities are as follows.

(a) If the velocity of the front is higher than 2.1 (± 0.6) μm s^{-1}, colloidal precipitate does not appear either near the reaction front, or behind it. This happens for example at the meeting point of two reaction fronts (Fig. 1b and c). If two reaction fronts moving toward each other meet, they form a single, connected front. In the proximity of the meeting point the front velocity is significantly higher, and a region free of brown precipitate remains after the reaction is complete (Fig. 1c). Note, that the highest front velocity measured was 12.5 μm s^{-1}.

(b) At slower reaction front velocities, in general between 0.9 and 1.8 μm s^{-1}, a brown colloidal precipitate emerges 7–8 min after the front has swept through the gel region (Fig. 1b) The brown colloid fills the space where the structureless precipitate was present (Fig. 1c). According to X-ray scattering experiments,[18] the brown compound is CuO. Note, that no colloidal precipitate is formed in the immediate proximity of the reaction front.

(c) If the velocity decreases further, a remarkable new phenomenon takes place. In contrast to the Liesegang phenomena, where the precipitation takes place behind a moving reaction front, here a homogeneously distributed colloidal precipitate, referred to from now as A-type precipitate, emerges just in front of the reaction zone (Fig. 1d). The site where the A-type precipitate is forming will be referred to from now as the front of the colloidal precipitation or colloidal front. Thus, the colloidal front precedes the reaction front. A possible explanation of this phenomenon is given in the Theoretical section.

Uniformly distributed A-type colloid was formed at front velocities between 0.6 and 0.9 μm s^{-1}. A few minutes later it decayed and was converted to the brown colloid (Fig. 1e). Note that in dark-field microscopic investigations the A-type precipitate shines in white, while the brown CuO one shines in a brown colour (Fig. 1f). A detailed investigation of the process of the formation of the A-type precipitate showed that it occurs in two steps. First, very small colloidal particles are formed, then these go through a ripening process.

(d) When the front velocity slows further, usually to 10–40 % below the value where the homogeneous A-type colloid first appeared, the precipitate starts to show a pattern (Fig. 2a): a regular structure of parallel stripes of colloidal precipitate appear approximately one wavelength distance in front of the reaction zone. At this stage, the dark-field investigations show clearly the dust of the small colloidal particles, which are the precursors of the A-type precipitate (Fig. 2d). Later these stripes are converted into brown stripes as CuO precipitate appears (Fig. 2b–c).

It is important to notice, that the wavelength of the secondary patterns is correlated with the velocity of the reaction front. Larger front velocity leads to smaller wavelength. The smallest wavelength observed was 15 μm, while the largest was 150 μm.

All the above effects can be seen in Fig. 3a: going from the upper to the lower part of the figure first regions free of colloidal precipitate, then homogeneous brown colloidal precipitate, and precipitate stripes of slightly growing wavelength can be observed. This sequence could be qualitatively reproduced by the computer simulations presented in the Theoretical section. Note, that at present the functional form of the connection between the front velocity and the wavelength of the pattern is unknown.

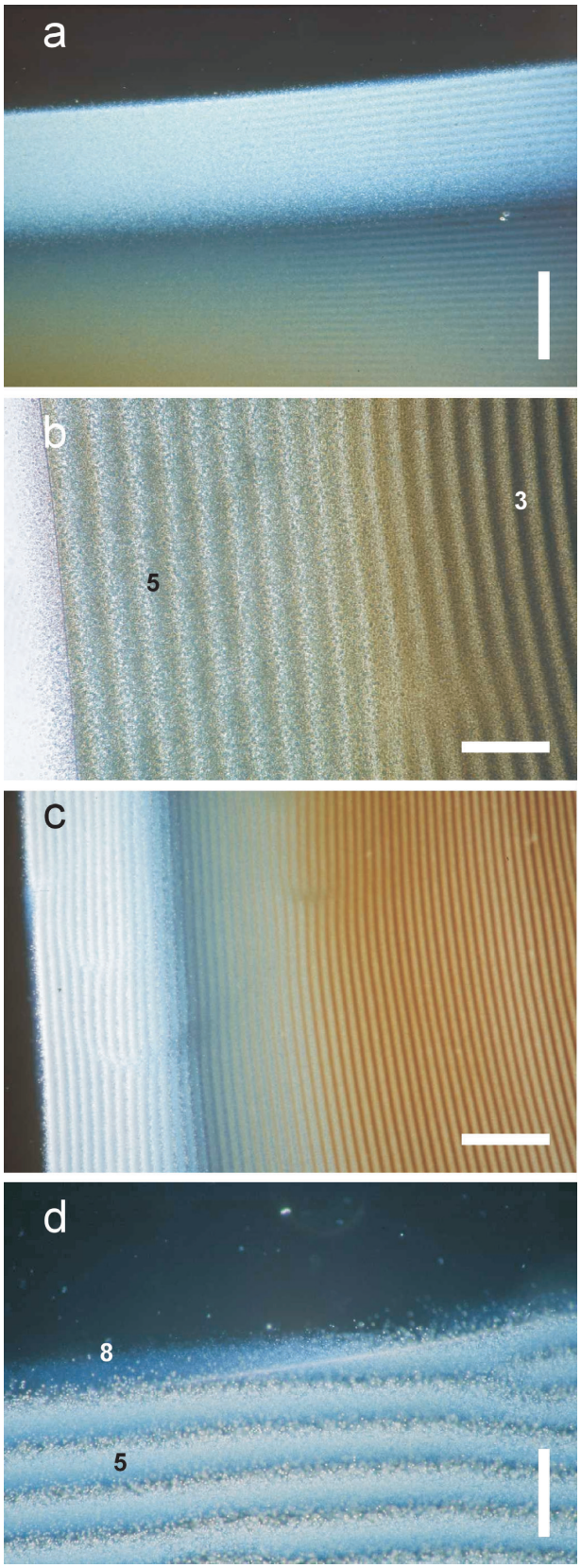

Fig. 2 (a) Dark-field investigation just when the A-type precipitate starts to show patterns. Scale bar = 200 μm. (b) Two main stages of the formation of the stripes of precipitates. The A-type precipitate (5) forms in the front of the reaction zone and transforms into a brown (3) one. Scale bar = 100 μm. (c) Similar patterns in dark-field investigation. Scale bar = 200 μm. (d) Dark-field investigation of the formation of a stripe. First a small-sized dust is formed at the colloidal front (8), which goes through a ripening process resulting in larger A-type colloids (5). Scale bar = 100 μm.

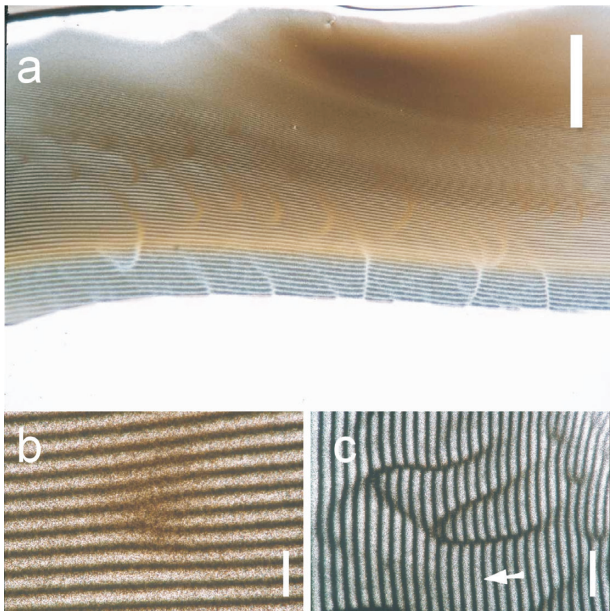

Fig. 3 (a) Development of a reaction front where several defects are also present. Scale bar = 800 μm. (b) Fork-like defect in a gel sheet. Scale bar = 50 μm. (c) Interactions of elongated defects: two defects forming successively closer to each other are annihilated, or only one of them survives. The arrow indicates the direction of the reaction front, which yield to this pattern. Scale bar = 200 μm.

Regular secondary patterns are not specific to a single chemical system. Their formation has also been observed in PVA gels without cross-linking. Emergence of similar regular grids has been observed in the NaOH + $AgNO_3$ reaction–diffusion system in PVA gel also. Note that in this case the minimal wavelength of the pattern is only 4 μm.

Increasing wavelength with decreasing front velocity is a characteristic feature of those chemical systems also, in which precipitation occurs behind a moving reaction front. This behaviour has been modelled by several systems of reaction–diffusion equations,[13–16] and by phase separation described by the Cahn–Hilliard equation.[22]

Defects in the secondary patterns

The secondary patterns, which are grids consisting of colloidal particles are not free of defects (Fig. 3a). An interesting dynamical feature of the reaction is the emergence and interactions of these defects. They usually appear when there are slight differences in the velocity between some parts of the reaction front. In most cases, the differences are not high enough to cause significant change in the wavelength of the grid, but the front segment having a greater velocity yields more precipitated stripes than the one with smaller velocity. If the wavelength is approximately constant, all the stripes cannot be continuous along the reaction front. At the front segment with higher speed new stripes are inserted, and fork-like errors are formed (Fig. 3b). Although several types of defects have been observed in chemical and physical systems,[23–26] the fork-like errors show most of the common features of defects present on the patterns of some sea shells, like those of *Nautilus pompilius*.[27] This animal bears a spiral-shaped shell, which results from a much faster growth on the periphery of the growing edge. The number of pigmented lines on the peripherial region is higher than along the inner side, and the interconnections of the pigmentation lines are usually similar to the fork-like errors presented above.

Another type of common error is the so-called elongated defect (Fig. 3c). If the distance between two elongated defects

growing toward each other decreases to about 2–3 wavelengths, an effective attractive interaction appears between them. After they meet, one or both of them will disappear (Fig. 3c). A possible explanation of this behaviour is given in the Theoretical section.

Experiments in gel columns

Formation of precipitate sheets instead of grids can also be achieved by having the reaction run in gel columns instead of gel sheets. In this case, the gel containing $CuCl_2$ is prepared in a test tube, NaOH solution is poured on the top, and thus a disk-like diffusion front is formed. Behind this front, formation of a large variety of primary patterns can take place, depending on the concentrations of the reactants.[18]

The velocity of the reaction front depends on the experimental set-up as well as on the reactant concentrations. Using 6.00 mL of 8.0 M NaOH solution as outer electrolyte and gel columns of 100–120 mm height, the secondary patterns (sheets of precipitate) appear only if the concentration of the $CuCl_2$ inner electrolyte is higher than about 0.7 M, because it has to be high enough to slow the front to the speed where the formation of the secondary patterns can occur. Unfortunately, at these concentrations, primary patterns are also present, so the sheets of the secondary, microscopic patterns are split by the primary ones. In order to obtain several hundreds of consecutive precipitate sheets, it is necessary to avoid the formation of the primary patterns.

If the concentration of $CuCl_2$ is lower than 1.11 ($\pm$ 0.05) M, the formation of the primary patterns can be suppressed. The suppression of the primary patterns can be achieved by decreasing the inner electrolyte concentration at the top region of the gel column by pouring an aqueous solution of HCl with pH 1.2 onto the gel, and keeping it there for 24 h before the reaction is started. Thus, when NaOH solution is poured on top of the gel column, the reaction front penetrates first into the gel region where the $CuCl_2$ concentration is not high enough for formation of the primary patterns, and homogeneous colloidal precipitate is formed.

After the front reaches the region 3–4 cm below the top of the gel column, where the concentration of the $CuCl_2$ has not been changed, and it is high enough to generate the primary patterns, these will not appear. This method of suppressing the primary precipitates does not work if the inner electrolyte concentration is higher than 1.11 ($\pm$ 0.05) M. Above this value, primary patterns emerge when the reaction front passes through the gel region with decreased $CuCl_2$ concentration. In ref. 18 a reverse phenomenon was reported. If the $CuCl_2$ concentration was in a range below a certain threshold, formation of the primary patterns could be achieved only by increasing the $CuCl_2$ concentration at the top of the gel column. Thus, a hysteresis-like behaviour is present in the system.

When the formation of the primary patterns is suppressed, in the above experimental set-up the secondary patterns appear when the concentration of the inner electrolyte is greater than about 0.8 M. The most regular sheets of precipitate are obtained with between 0.87 M and 0.96 M $CuCl_2$ (Fig. 4a and b). Although the wavelength of the patterns increases slightly as the velocity of the reaction front decreases, in this experimental set-up this effect can be neglected on the length of 1–2 cm, containing several hundred sheets of precipitate. Note, that the speed of the reaction front, and thus the wavelength can be kept constant if the outer electrolyte is continuously refreshed.

The system of precipitate sheets has large regions free of defects only inside a cylinder of 3–4 mm diameter in the centre of the gel column. Outside this region the wavelength decreases slightly as the radius increases, and therefore, fork-like errors, sometimes in an ordered hexagonal or cubic lattice, appear.

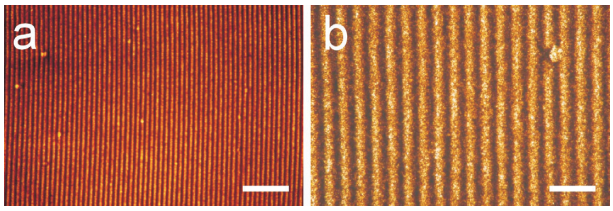

Fig. 4 Cross-sections of systems of equidistant precipitate sheets at different magnifications. The difference in the shade of the colours is due to the different thickness of the samples. (a) The concentration of the outer electrolyte was 8.0 M, while that of the inner electrolyte was 0.966 M. Scale bar = 200 μm. (b) The concentration of the outer electrolyte was 8.0 M, while that of the inner electrolyte was 0.879 M. Scale bar = 50 μm.

This is probably caused by the syneresis of the gel. Syneresis is also responsible for the nonplanar shape of the reaction front, which is slightly concavely curved looking from the gel surface, causing a slight distortion of the precipitate sheets. These errors can be reduced by using larger test tubes.

Theoretical

At the present stage of research the mechanism of pattern formation is mostly unknown, and thus, possible mathematical models can be deduced only by phenomenological assumptions. Our aim was to construct a dimensionless model which reproduces the following most important features of the formation of the precipitate stripes: (i) they form in front of the reaction zone, *i.e.* the colloidal front precedes the reaction front, (ii) their wavelength decreases as the speed of the reaction front increases, and (iii) the precipitated zones have about the same width as the empty spaces in between.

A mathematical model was elaborated that reproduces these features of the experiments in certain parameter domains. It was assumed that the moving reaction front produces a chemical, which acts as the substrate for the formation of the colloidal stripes. This substrate has to reach a critical concentration to start the production of a compound which may correspond to the colloidal dust, which is the precursor of the A-type colloidal precipitate. The advancing of the reaction front and details of the substrate production can also be modelled by reaction-diffusion equations,[19] but in the interests of simplicity it will be encoded directly into the models.

Formation of the patterns occurs as follows. Let us assume, that the concentration of the substrate is high enough in a region located in front of the reaction zone, and thus, formation of the species corresponding to the colloidal dust precursor of the A-type precipitate is taking place.

The substrate concentration at which the formation of this species, supposed to be a primary reaction product, starts is referred to as the 'nucleation threshold'. Ripening processes are also taken into account: the primary reaction product has a small, but nonzero diffusion rate, and decays to a final, non-diffusible product, corresponding to the A-type precipitate. Note that the model does not describe further conversions of this compound. Once the final precipitate appears, the substrate can precipitate directly on it, and this process is proportional to the concentration of the substrate and that of the final precipitate, and does not need any thresholds. The accumulation of the products is suppressed by a saturation term.

In this model production of the primary and the final reaction products is assumed to be accompanied by the formation of an inhibitor. If the inhibitor is present, the nucleation threshold is higher. Therefore, after the formation of a stripe of the final reaction product, nucleation in its surroundings is prohibited. But, as the reaction front goes

through and leaves the precipitated region, the concentration of the substrate increases over a large region ahead of the reaction front. If this region overlaps the area where nucleation cannot take place due to the high inhibitor concentration, then formation of the new stripe will take place ahead of the reaction front, outside the inhibited area. Zero flux boundary conditions are assumed for all compounds involved in the model.

Experimental observations by optical microscope indicated that after the reaction front has swept through a gel region, *i.e.* after that region has been filled with the structureless precipitate which is green in transmitted light, nucleation and colloidal growth are no longer taking place. This effect was taken into account by switching to zero the appropriate reaction rates behind the reaction front.

The equations comprising this model are the following:

$$a(x,t) = \sigma(x - vt) \tag{1a}$$

$$\frac{\partial s(x,t)}{\partial t} = D_s \frac{\partial^2 s(x,t)}{\partial x^2} + r_0 \sigma(x - vt) - F_1 - F_2 \tag{1b}$$

$$\frac{\partial h(x,t)}{\partial t} = D_h \frac{\partial^2 h(x,t)}{\partial x^2} + r_3(F_1 + F_2) \tag{1c}$$

$$\frac{\partial p_1(x,t)}{\partial t} = D_{p_1} \frac{\partial^2 p_1(x,t)}{\partial x^2} + F_1 - \gamma p_1(x,t) \tag{1d}$$

$$\frac{\partial p(x,t)}{\partial t} = \gamma p_1(x,t) + F_2 \tag{1e}$$

where

$$F_1 = \frac{r_1(x,t)\theta(s(x,t) - U(x,t))}{Q(x,t)} \tag{2a}$$

$$F_2 = \frac{r_2(x,t)s(x,t)p(x,t)}{Q(x,t)} \tag{2b}$$

$$U(x,t) = k_1(1 + k_2 h^2(x,t)) \tag{2c}$$

$$Q(x,t) = 1 + k_3(p_1(x,t) + p(x,t))^2 \tag{2d}$$

The reaction front $a(x,t)$ is represented by the sharp source term σ, which moves ahead with speed v (eqn. (1a)). In computer simulations, the function σ has unit height and its width is equal to the mesh size. The concentration of the substrate $s(x,t)$ evolves in time according to eqn. (1b). This compound, having initial condition $s(x,0) = 0$ and diffusion rate D_s, is produced by the reaction front with rate r_0. The concentration of the substrate is reduced by two processes, denoted by the terms F_1 and F_2.

F_1 represents the formation of the primary reaction product $p_1(x,t)$ ('nucleation'), while F_2 the 'growth' of the final product $p(x,t)$. Initial conditions for these compounds are $p_1(x,0) = 0$ and $p_2(x,0) = 0$. Formation of the primary product occurs when the argument of the Heaviside function θ in eqn. (2a) becomes positive, that is when the substrate concentration overtakes the inhibition caused by $h(x,t)$. The inhibition of the nucleation, represented by $U(x,t)$, which can be tuned by the reaction constants k_1 and k_2, is assumed to grow quadratically with the inhibitor concentration (eqn. (2c)). Term F_2 is supposed to be linear in $s(x,t)$ and $p(x,t)$ (eqn. (2b)).

Similar expressions to those in the nominators of F_1 and F_2 are widely used in the modelling of colloidal nucleation and growth, respectively.[14,15] Saturation of products is represented by the quadratic term $Q(x,t)$ in the denominators of the fractions F_1 and F_2 (eqn. (2d)). Such saturation terms are well known in mathematical models of pattern formation.[27]

The reaction rates, $r_1(x,t)$ and $r_2(x,t)$, are constant values (r_1 and r_2, respectively) ahead of the reaction front and are zero behind it. The latter can be justified by the experimental results mentioned above, *i.e.* the formation of the products is halted behind the reaction front.

Primary reaction product $p_1(x,t)$ is generated through 'nucleation' represented by the term F_1. This compound has a small diffusion coefficient D_{p_1}, and decays into $p(x,t)$ with rate γ (eqn. (1d)). The final product, formed either by decay of $p_1(x,t)$, or by the 'growth' described by F_2, is unable to diffuse (eqn. (1e)). The increase of the inhibitor $h(x,t)$ having diffusion coefficient D_h is proportional to the formation of the reaction products (eqn. (1c)). The coefficient of proportionality is r_3.

In order to understand the properties of the reaction–diffusion system described by eqn. (1) and (2), computer simulations were carried out by numerical integration of these equations with simple time marching. Spatial discretization was performed with the finite difference scheme in a one-dimensional segment of length $L = 6500$. The mesh size was $\Delta x = 0.1$, and the time step $\Delta t = 0.0001$. No significant change in the simulation results was observed when the time step and the mesh size were halved. Simulation results representing the wavelength of the emerging pattern *vs.* the speed of the reaction front are plotted in Fig. 5a. The wavelength of the striped patterns obtained by the computer simulations is defined as the distance between the points of maximum concentration of the final reaction product $p(x,t)$, having passed the transient period at the beginning of the diffusion column.

The striped reaction product appeared only when the speed of the reaction front was below about $v = 2$. As the speed of the reaction front was increased, homogeneous 'precipitation', and finally, front propagation without the production of $p(x,t)$ was observed, in complete agreement with the experiments.

Fig. 5b shows the concentration profile of product $p(x,t)$ and the position of the front itself when the formation of a new stripe has just begun, at the front speed $v = 1$. It can be observed that this happens roughly when the reaction front overtakes the last stripe of the reaction product.

We mention that the patterns seen in the simulations are stable in a certain range of parameters. No qualitative change was observed when the parameters of Fig. 5a were varied by $\pm 15\%$.

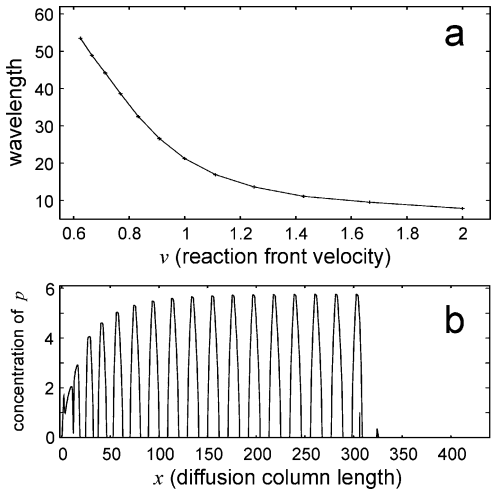

Fig. 5 Simulation results. All units are dimensionless. (a) Dependence of the striped pattern's wavelength on the velocity of the reaction front. Parameters: $D_s = 16$, $D_h = 6$, $D_{p_1} = 0.04$, $r_0 = 8$, $r_1 = 1$, $r_2 = 1$, $r_3 = 2$, $k_1 = 1$. $k_2 = 1$, $k_3 = 3$, $\gamma = 4$. (b) Concentration profile of the reaction product $p(x,t)$ at the parameters as in (a), and reaction front speed $v = 1$. The reaction front is represented by the sharp peak in the last developed stripe, at $x \approx 305$. The formation of a new stripe has just begun ahead of the reaction front, at $x \approx 325$.

One of the main interests in the experiments on these pattern forming reactions is to obtain regular grids with smaller, submicrometric wavelength. Several ways led to a decrease in the wavelength in the computer simulations. A simple, and experimentally also reasonable, possible way of doing this is to decrease the diffusion coefficients, while maintaining their ratio constant.

The model described above leads to an interpretation of the effective attractive interaction that acts between two defects which are closer than 2–3 wavelengths. The main feature of this phenomenon is the vanishing of the precipitate stripe which forms in between the elongated-type defects (Fig. 3a and c). This can be explained by the gradual overlap of the regions where inhibitor concentration is high, and substrate concentration is low due to the stripes formed on the outer parts of the defects.

Other classes of models that also reproduce the main features of the formation of the stripes of precipitates have been elaborated and studied by computer simulation. Thus, further experiments are required in order to find out the real pattern forming mechanism. Although all of these models are rather *ad hoc*, their common basic elements and their qualitative accordance with the experimental results may help researchers to find out the mechanism of the reaction. The most important feature of the models is that a species necessary for the process of building up the colloidal stripes is formed in the reaction front.

Note, that the substrate which is assumed in the model presented above is probably not the diffusive intermediate proposed in the explanation of the primary patterns,[19] because formation of the precipitated stripes does not seem to affect the dynamics and shape of the reaction front.

Possible technological applications

The most important new property of the experimental systems presented here is their ability to yield regular patterns even under 20 μm despite the simple reagents. Elucidation of the detailed reaction mechanism and further study of reactions of this type may lead to new techniques in several industrial processes. A promising application of the gels filled with periodic sheets of precipitate would be in the manufacture of optical gratings.[28,29] Gratings prepared by the sectioning of gel columns which contained equidistant sheets of precipitate have been tested successfully. Another possibility is an alternative method of production of 1D photonic crystals, which consist of periodically layered materials having different dielectric constants.[30–32] Composite materials similar to those presented here are required in several technological processes.[33]

Acknowledgements

I am indebted to Z. Rácz, T. Turányi, E. Szathmáry, E. Kőrös, V. Gáspár, T. Perger, I. László and A. Büki for useful discussions; G. Zboray, A. Magyar, N. Nagy, Zs. Maglóczky, I. Jalsovszky, J. Rábay, Z. Gy. Horváth, K. Kamarás and A. Varga for their help in some experiments; to I. Oláh (Semmelweis University, Dept. of Human Morphology and Developmental Biology), M. Orbán (Eötvös University, Dept. of Analytical Chemistry) and M. Sass (Eötvös University, Dept. of General Zoology) for the opportunity to work in their departments. I acknowledge the support of G. Kéri, E. Keszei, L. Szilágyi, L. Gráf, K. Szabó, G. Inzelt, T. Kornay, the Hungarian Ministry of Education, and the Hungarian Research Funds (Grant OTKA T029792). Most of the computer simulations were performed on the Compaq Alpha Supercomputer of Eötvös University, Center for Information Technologies. Additional details are available from the author on request (hantz@poe.elte.hu or hantz@ludens.elte.hu).

References

1 I. R. Epstein and K. Showalter, *J. Phys. Chem.*, 1996, **100**, 13 132.
2 S. K. Scott, *Oscillations, Waves and Chaos in Chemical Kinetics*, Oxford University Press, Oxford, 1995.
3 I. R. Epstein and J. A. Pojman, *An Introduction to Nonlinear Chemical Dynamics*, Oxford University Press, New York, 1998.
4 S. C. Müller and M. J. B. Hauser, in *Handbook of Biomimetics*, ed. Y. Osada, S. Kai, Y. Kakazu, K. Kataoka, K. Sakai and J. Tanaka, NTS Books, Tokyo, 2000, p. 87.
5 H. L. Swinney and V. I. Krinsky, *Waves and Patterns in Chemical and, Biological Media*, MIT/North-Holland, Cambridge, MA, 1991.
6 P. K. Maini, K. J. Painter and H. Nguyen Phong Chau, *J. Chem. Soc., Faraday Trans.*, 1997, **93**, 3601.
7 J. A. Murray,*Mathematical Biology*, Springer, Berlin, 1993.
8 L. Wolphert, *Principles of Development*, Oxford University Press, Oxford, 1998.
9 A. Lázár, H.-D. Försterling, H. Farkas, P. Simon, A. Volford and Z. Noszticziusz, *Chaos*, 1997, **7**, 731.
10 á Tóth, V. Gáspár and K. Showalter, *J. Phys. Chem.*, 1994, **98**, 522.
11 P. W. Davies, P. Blanchedeau, E. Dulos and P. De Kepper, *J. Phys. Chem. A*, 1998, **102**, 8236.
12 J. Schütze, O. Steinbeck and S. C. Müller, *Nature*, 1992, **356**, 45.
13 H. Henish, *Crystals in Gels and Liesegang Rings*, Cambridge University Press, Cambridge, 1988.
14 T. Antal, M. Droz, J. Magnin, Z. Rácz and M. Zrínyi, *J. Chem. Phys.*, 1998, **109**, 9479.
15 A. Büki, É. Kárpáti-Smidróczki and M. Zrínyi, *J. Chem. Phys.*, 1995, **103**, 10 387.
16 T. Antal, M. Droz, J. Magnin and Z. Rácz, *Phys. Rev. Lett.*, 1999, **83**, 2880.
17 A. A. Kodentsov, M. H. J. van Dal, C. Cserháti, A. M. Gusak and F. J. J. van Loo, *Defect Diffusion Forum*, 2001, **194–199**, 1491.
18 P. Hantz, *J. Phys. Chem B*, 2000, **104**, 4266.
19 P. Hantz, to be published.
20 Zs. Nagy-Ungvárai, A. M. Pertsov, B. Hess and S. C. Müller, *Physica D*, 1992, **61**, 205.
21 P. Grindrod, *The Theory and Applications of Reaction-Diffusion Equations. Patterns and Waves*, Clarendon Press, Oxford, 1996.
22 F. De Pasquale and Z. Rácz, to be published.
23 M. C. Cross and P. C. Hohenberg, *Rev. Mod. Phys.*, 1993, **65**, 851.
24 Q. Quiang and J.-M. Flesselles, *Nature*, 1996, **379**, 143.
25 M. Bär, M. Falcke and M. Or-Guil, in *Transport and Structure: Their Competitive Roles in Biophysics and Chemistry*, ed. S. C. Müller, J. Parisi and W. Zimmermann, Springer Lecture Notes in Physics, vol. 532, Berlin, 1999, p. 326.
26 Yu. A. Astrov, E. Ammelt and H.-G. Purwins, *Phys. Rev. Lett.*, 1997, **78**, 3129.
27 H. Meinhardt, *The Algorithmic Beauty of Sea Shells*, Springer, Berlin, 1995.
28 H. Nishihara, M. Haruna and T. Suhara, *Optical Integrated Circuits*, McGraw-Hill, New York, 1989.
29 J. Rantala, *Sol-Gel Materials for Photonic Applications*, VTT, Espoo, 1998.
30 J. D. Joannopoulous, P. R. Villeneuve and S. Fan, *Nature*, 1997, **386**, 143.
31 J. D. Joannopoulos, R. D. Meade and J. N. Winn, *Photonic Crystals*, Princeton University Press, Princeton, 1995.
32 J. M. Rowell, *Sci. Am.*, 1986, **255**, 124.
33 Y. Xia, B. Gates, Y. Yin and Y. Lu, *Adv. Mater.*, 2000, **12**, 693.